

A Novel Asymmetric-Magnetic-Pole Interior PM Machine With Magnet-Axis-Shifting Effect

Hui Yang^{ID}, Senior Member, IEEE, Cheng Qian^{ID}, Weijia Wang, Heyun Lin^{ID}, Senior Member, IEEE, Z. Q. Zhu^{ID}, Fellow, IEEE, Shuangxia Niu^{ID}, Senior Member, IEEE, Wei Liu^{ID}, and Shukang Lyu^{ID}

Abstract—This article proposes a novel asymmetric-magnetic-pole interior permanent magnet (AMP-IPM) machine, which is geometrically characterized by a combination of dual-layer reluctance and flat-type PM rotor structures. The design concept of “asymmetric-magnetic-pole” is introduced to achieve a magnet-axis-shifting effect, namely, the magnet d -axis is shifted to make PM and reluctance torque components approximately maximize at similar current angles. Consequently, the resultant torque can be further improved without increasing magnet usage. The machine topology is first introduced. The electromagnetic characteristics of the proposed AMP-IPM machine are then investigated and compared with those of the benchmark conventional IPM machine with symmetrical magnetic poles, with similar sizing and PM usage. Finally, an AMP-IPM machine prototype is manufactured and tested, which confirms the feasibility of the proposed AMP design for the torque performance improvement.

Index Terms—Asymmetric-magnetic-pole, interior permanent magnet (IPM), magnet-axis-shifting (MAS), magnet torque, reluctance torque.

I. INTRODUCTION

PERMANENT MAGNET (PM) machines [1]–[5] are of growing research interest in the last decade. Due to their distinctive merits of high power/torque density, high efficiency,

Manuscript received February 1, 2021; revised May 19, 2021; accepted August 31, 2021. Date of publication September 13, 2021; date of current version November 19, 2021. This work was supported in part by the National Natural Science Foundations of China under Grants 52077033 and 52037002, in part by the Fundamental Research Funds for the Central Universities under Grant 2242017K41003, in part by the “Zhishan Youth Scholar” Program of Southeast University, in part by the Jiangsu Provincial Key Laboratory of Smart Grid Technology and Equipment, Southeast University under Grant 7716008046, and in part by the Excellence Project Funds of Southeast University.” Paper 2021-EMC-0082.R1, presented at the 2019 IEEE International Electric Machines & Drives Conference, San Deigo, CA, USA, May 12–15, and approved for publication in the IEEE TRANSACTIONS ON INDUSTRY APPLICATIONS by the Electric Machines Committee of the IEEE Industry Applications Society. (Corresponding author: Hui Yang.)

Hui Yang, Cheng Qian, Weijia Wang, Heyun Lin, Wei Liu, and Shukang Lyu are with the School of Electrical Engineering, Southeast University, Nanjing 210096, China (e-mail: huiyang@seu.edu.cn; seueelab_qc@163.com; seueelab_wwj@163.com; hyling@seu.edu.cn; seueelab_lw@163.com; seueelab_lsk@163.com).

Z. Q. Zhu is with the Department of Electronic and Electrical Engineering, University of Sheffield, S1 3JD Sheffield, U.K. (e-mail: z.q.zhu@sheffield.ac.uk).

Shuangxia Niu is with the Department of Electrical Engineering, The Hong Kong Polytechnic University, Hong Kong (e-mail: eesxniu@polyu.edu.hk).

Color versions of one or more figures in this article are available at <https://doi.org/10.1109/TIA.2021.3111153>.

Digital Object Identifier 10.1109/TIA.2021.3111153

and expedient maintenance, PM machines were widely commercialized in various industry applications [1]–[4], e.g., electric vehicles, marine propulsion, domestic appliances, and wind power generation, etc. Amongst PM machines, interior permanent magnet (IPM) machine with PMs buried inside the rotor core can effectively utilize the reluctance torque to enhance the overall torque density resulting from the difference of d - and q -axis magnetic circuits. Thus, the IPM machines are preferred in applications, which require excellent flux-weakening capability with a wide constant power speed range (CPSR), as well as good rotor magnet protection [5]–[7].

For the existing IPM machines [8]–[25], the magnet and reluctance torques reach the maximum values at different current angles, so that the resultant torque only uses a portion of either the magnet torque or the reluctance torque. Thus, it is highly desirable to improve the utilization ratio of individual torque component. On the other hand, the rising price and limited availability of rare-earth magnet materials also increase the demands to develop various IPM machines with reduced rare-earth material or high magnet torque utilization ratio [6]. In order to address the above issues, the PM-assisted synchronous reluctance machines [9], [10] are widely recognized as one of the effective countermeasures to further improve the reluctance torque, and consequently the magnet usage can be reduced correspondingly. In this case, the rotor is designed with higher numbers of magnet cavity layers in each rotor pole to generate a high saliency ratio. Nonetheless, these machines still suffer from high torque ripple, complicated magnet retaining, and mechanical vibration issues [9]. Besides, the multilayer flux barrier may lead to considerable PM flux leakage, limited d -axis flux and significant cross-coupling effect. In addition to the structure drawbacks, the nature of this type of machine results in the mismatch of PM magnetic and reluctance axes, which results in the low utilization ratios of both components in the maximum resultant torque. Accordingly, two design concepts are proposed by using asymmetric magnetic pole structure to shift the peak points of PM and reluctance torque components with reference to the current angle to be closer, so as to improve the average torque with the same PM usage, which are designated as reluctance axis shifted (RAS) effect [11]–[16] and magnet-axis-shifting (MAS) effect [20]–[25].

In [12]–[16], several possibilities to realize a synchronous machine with displaced reluctance axis have been discussed. Furthermore, a hybrid PM and wound field synchronous machine [12] with a displaced reluctance axis is proposed, which is known for improving motor operation performance

and efficiency at the cost of an inferior generator operation. A reluctance axis shifted effect is proposed by employing additional airspace beside the magnet in the cases of many IPM machines [13]–[16], resulting in that the reluctance axis shifts closer to the magnet axis. As a result, the optimal current angles for maximizing the two torque components are approximately equal. Other solutions for achieving this objective refer to hybrid rotor machine [17], [18] and dual rotor machine [19], which commonly utilizes two independent rotor parts providing reluctance and magnet torque components, respectively. Thus, the two rotors can be displaced to unify the optimal current angles for reluctance and magnet torques.

On the other hand, various asymmetric IPM (AIPM) rotor topologies based on MAS effect for the torque performance improvement are developed [20]–[25]. In [22], a novel asymmetric IPM rotor topology-featured additional rotor slots as well as unequal magnet widths within one magnetic pole, is proposed for electric vehicle applications. Besides, a novel spoke-type asymmetric IPM machine [23] is introduced by employing spoke-type symmetrical PMs and asymmetric flux barrier structure. In addition, a hybrid PM machine characterized by a different magneto-motive-force distribution is developed to achieve a MAS effect. All above solutions [20]–[24] aim to utilize the MAS effect for torque enhancement by reducing the current angle difference between peak PM and reluctance torque components, thereby effectively increasing the maximum resultant torque. Nevertheless, the difference between the optimal current angles for the magnet and reluctance torques for the existing asymmetric IPM machines is still relatively large, which is undesirable for the overall torque enhancement.

Therefore, this article proposes a novel design of asymmetric-magnetic-pole IPM (AMP-IPM) machine with an asymmetric magnet configuration [25], which is the combination of the dual-layer reluctance and flat-type PM rotor structures. The main advantage of the proposed machine is the torque density enhancement due to the asymmetric PM configuration. Thus, the proposed machine is quite suitable for cost-sensitive applications requiring high torque-to-magnet-usage ratio, such as wind power generation, electric vehicle, domestic, and other aspects. The design concept of “asymmetric-magnetic-pole” is introduced to achieve an MAS effect, namely, the magnet *d*-axis can be shifted to make PM and reluctance torque components approximately maximize at similar current angles, further improving the resultant torque without increasing magnet usage. The machine structures and MAS mechanism are introduced, respectively. Furthermore, the electromagnetic characteristics of the AMP-IPM machine are investigated and compared with those of the referenced conventional IPM machine. Finally, some experiments are carried out on an AMP-IPM machine prototype, which verifies the feasibility of the proposed design for the torque performance improvement.

II. MACHINE TOPOLOGIES AND MAS EFFECT

A. Structure of Proposed MAS-IPM Machine

The configurations of the conventional IPM machine having three reluctance layers and the proposed AMP-IPM machine

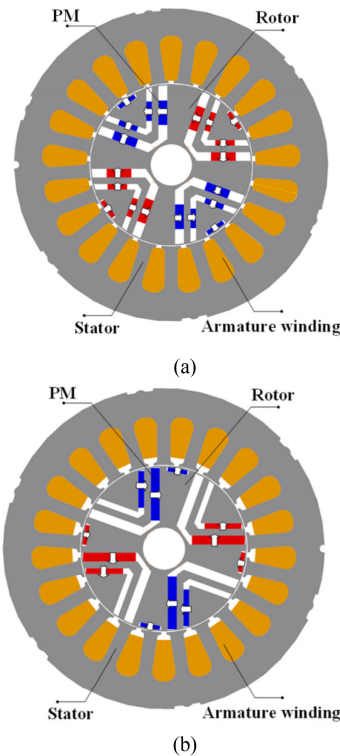


Fig. 1. IPM machine topologies. (a) Conventional IPM machine. (b) Proposed AMP-IPM machine.

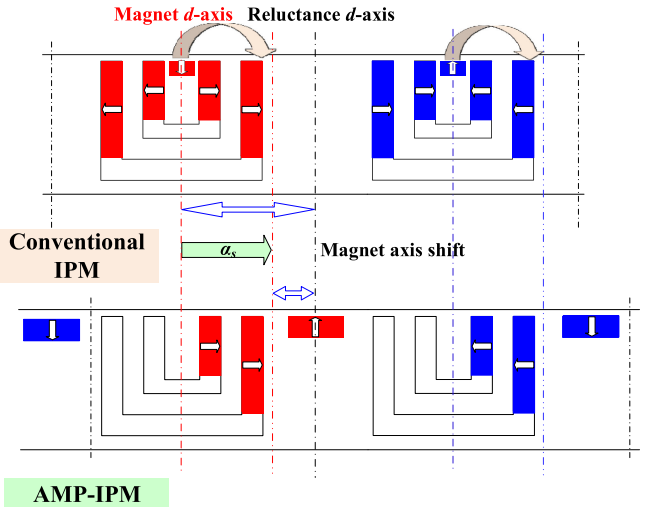


Fig. 2. Illustration of topology evolution and magnet-axis-shifting principle of the proposed AMP-IPM machine.

are shown in Fig. 1. Both machines employ a 21-slot/4-pole fractional-slot distributed winding and the same stator structure. Besides, the airspace barrier structure, magnet usage, as well as the overall sizing are identical for the two cases so as to perform a fair comparison. The corresponding principle of the topology derivation is illustrated in Fig. 2. It demonstrates that the proposed AMP-IPM machine can be obtained by shifting the flat-type magnet at the upper side of the traditional one to the central position between two adjacent reluctance parts. The PMs located on the left side of the air-gap barriers are removed,

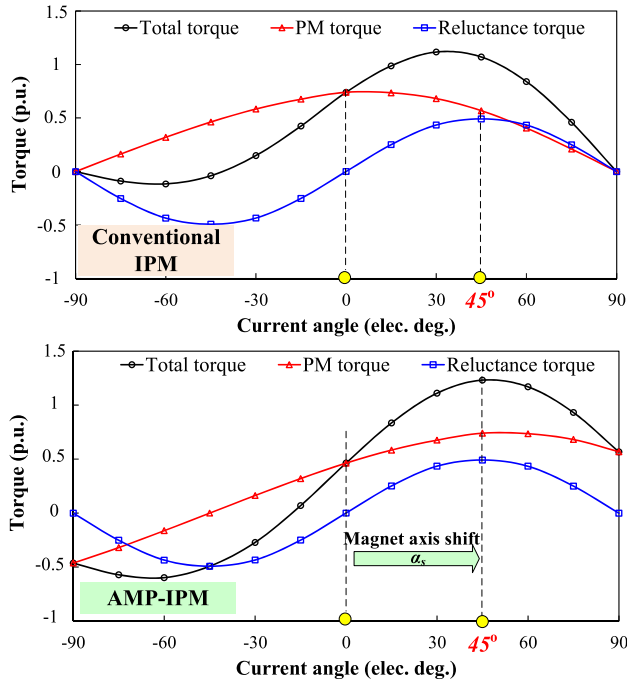


Fig. 3. Torque improvement principle of the proposed AMP-IPM machine.

resulting in an asymmetric hybrid magnet pole arrangement. The proposed AMP-IPM design can offer multiple degrees-of-design flexibility due to the hybrid nature of different PM pole structures. Meanwhile, the torque capability can be further improved by aligning the magnet torque with the reluctance torque due to the MAS effect.

B. Magnet-Axis-Shifting Effect

Generally, the electromagnetic torque equation of the IPM machine can be governed by [6]

$$T_{\text{total}} = T_{PM} + T_r = \frac{3}{2} p_r \psi_f i_s \cos \beta + \frac{3}{4} p_r (L_d - L_q) i_s^2 \sin 2\beta \quad (1)$$

where T_{total} , T_{PM} , and T_r are the total torque, the magnet torque, and the reluctance torque, respectively; p_r , ψ_f , i_s , and β are the rotor pole pair, the PM flux linkage, the phase current, and the current angle, respectively; L_d and L_q are the d - and q -axis inductances, respectively.

It can be observed from (1) that the total torque contains two components. The first one is T_{PM} , which is produced by the interaction between ψ_f and i_s , and the second one is T_r owing to the difference in d - and q -axis inductances ($L_d - L_q$). As conventional IPM machines usually have symmetrical rotor structure, the PM and reluctance torque components inherently reach maximum points at different current advancing angles whose difference is theoretically 45 electrical degrees (ED), as shown in Fig. 3. This reduces utilization ratios of both torque components at maximum resultant torque point. The proposed AMP-IPM machines have an asymmetric magnet arrangement, which shifts the position of the magnet d -axis, as shown in Fig. 4,

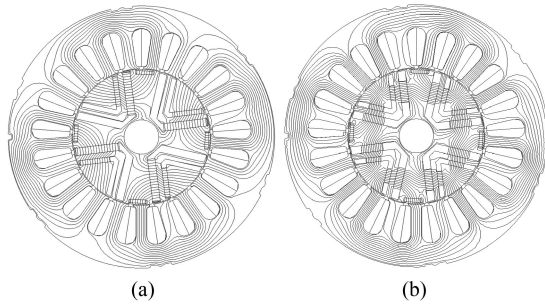


Fig. 4. Open-circuit field distributions. (a) Proposed AMP-IPM machine. (b) Alternate AMP-IPM machine.

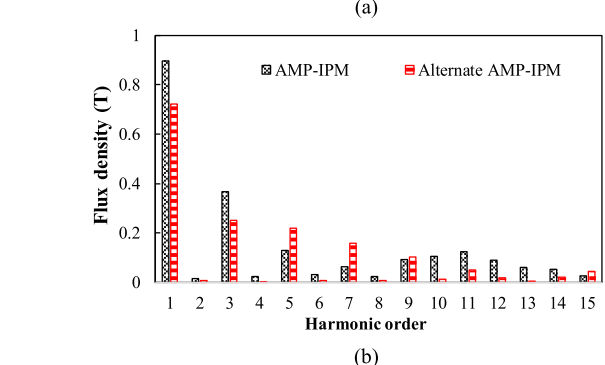
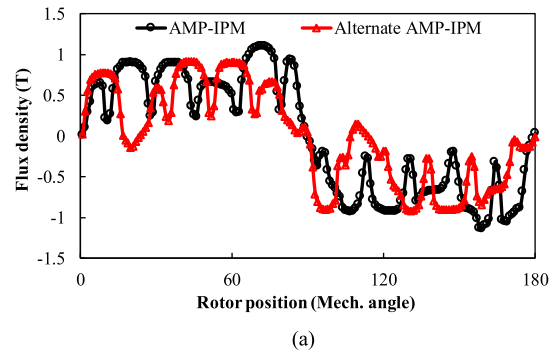


Fig. 5. Open-circuit air-gap flux density. (a) Waveforms. (b) Harmonic spectra.

thereby reducing the current angle difference between maximum PM and reluctance torque components. It is designated as magnet-axis-shifting (MAS) effect in this article [25].

The torque improvement mechanism of the proposed AMP-IPM machine is illustrated in Fig. 5. It can be observed that the magnet axis displacement is achieved by employing the AMP-IPM design concept and asymmetric PM structure. As a consequence, the corresponding torque equation of the AMP-IPM machine can be rewritten as

$$T_{\text{total}} = T_{PM} + T_r = \frac{3}{2} p_r \psi_f i_s \cos (\beta + \alpha_s) + \frac{3}{4} p_r (L_d - L_q) i_s^2 \sin 2\beta \quad (2)$$

where α_s denotes the shift angle of the magnet axis. Thus, it can be theoretically derived from (2) that as α_s satisfies " $\alpha_s = \beta$," the optimum current angle when the magnet torque peaks is accordingly aligned with that for the reluctance torque, resulting in the improvement of the total torque.

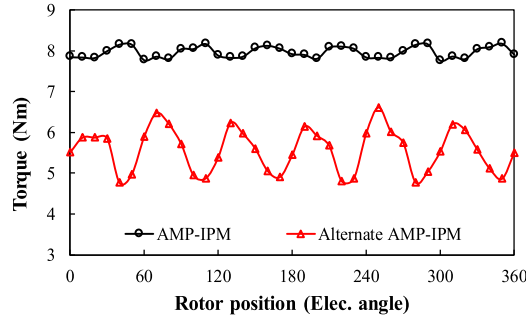


Fig. 6. Comparison of steady-state torque waveforms @ MTPA operation.

III. DESIGN AND ELECTROMAGNETIC PERFORMANCE

A. Magnet Type Selection

In order to select a proper magnet configuration, two possible changes from the original IPM machine are presented in Fig. 4: 1) The flat-type magnets are shifted to the central position between two adjacent reluctance parts; 2) the magnets in the flux gaps are moved to one side. The corresponding open-circuit field distribution of the alternate AMP-IPM machine (without the second change) is shown in Fig. 4(b). It can be observed that the magnetic circuit as well as the main flux path becomes longer in the case of alternate AMP-IPM machine due to the increased magnet pieces when changing the position of the magnets. Meanwhile, the flux plot patterns and the positions of the magnet d -axis axes for the two AMP-IPM cases are quite different. The corresponding open-circuit air-gap flux density waveforms of the proposed and the alternate AMP-IPM machines are shown in Fig. 5. It shows that the alternate AMP-IPM machine produces less fundamental air-gap flux density than that of the proposed machine, producing lower torque under loaded operation, as reflected in Fig. 6. From the torque against current angle characteristics of AMP-IPM machines with different PM designs in Fig. 7, it shows that the optimal phase current angles for the magnet and reluctance torques of the alternate AMP-IPM machine is different. That is to say, the MAS effect is inconspicuous without the second change, resulting in the torque capability lower than the proposed machine, as can be also represented in Fig. 4.

B. Design Optimization

In order to confirm the advantages of the proposed AMP-IPM machine design, its electromagnetic characteristics are compared with those of the conventional IPM machine.

The multiobjective genetic algorithm (GA) embedded in JMAG 19.1 software package is employed to optimize the torque quality with the constraints of the overall dimensions, the slot packing factor of 0.5, and the rated current density of 6.5 A/mm^2 . The geometric parameters are defined in Fig. 8, and their corresponding scopes are listed in Table I. All the design variables are globally optimized with multiobjective genetic algorithm, which can be employed to achieve an optimum design without considering the optimization sequence. Meanwhile, the

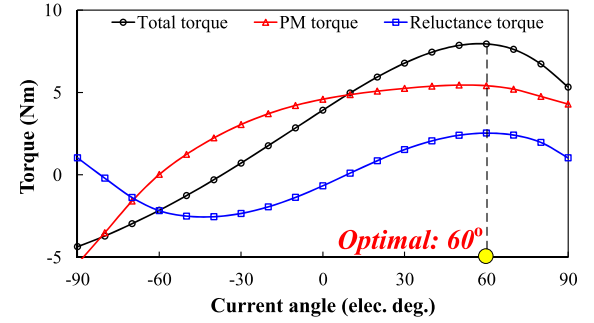


Fig. 7. Torque against current angle curves. (a) Proposed AMP-IPM machine. (b) Alternate AMP-IPM machine @ 7.5 A.

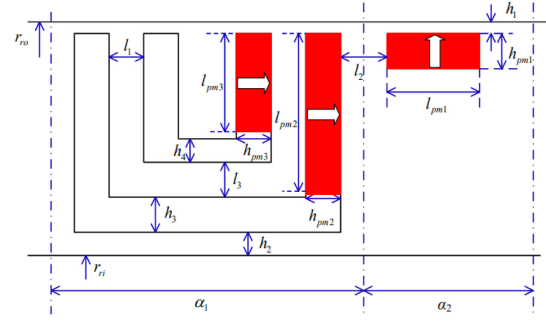


Fig. 8. Illustration of design parameters of the proposed AMP-IPM machine.

TABLE I
OPTIMIZING CONSTRAINTS

Parameter	Unit	Range
l_{pm1}	mm	4~14mm
h_{pm1}	mm	1.5~3mm
l_{pm2}	mm	16~21mm
h_{pm2}	mm	2.5~3.5mm
l_{pm3}	mm	10~15mm
h_{pm3}	mm	1.8~2.8mm
α_1	mm	25~35deg
l_1	mm	1~3.5mm
l_2	mm	0.5~3.5mm
l_3	mm	2~6mm
h_3	mm	1~3mm
h_4	mm	1~3mm

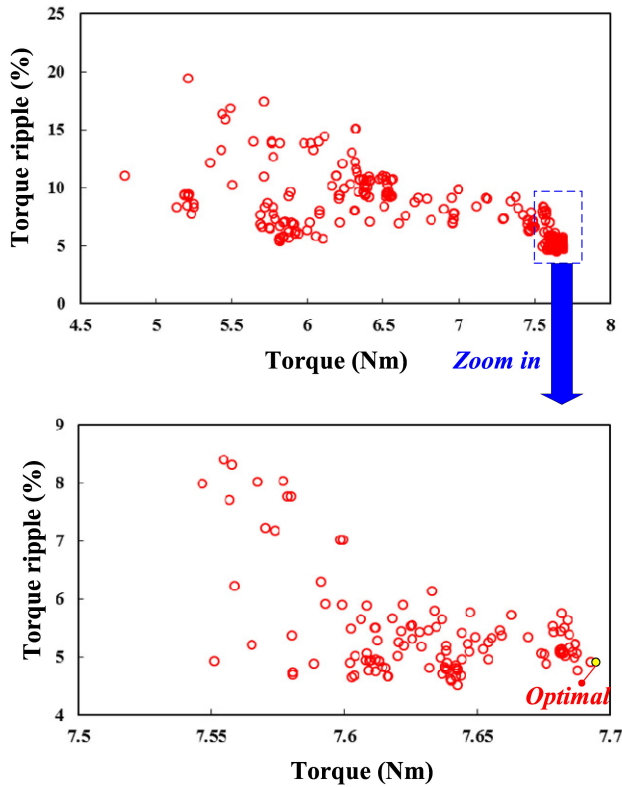


Fig. 9. Global optimization results of the proposed AMP-IPM machine.

TABLE II
MAJOR DESIGN PARAMETERS OF CONVENTIONAL IPM AND PROPOSED
AMP-IPM MACHINES

Items	Unit	Conventional	Proposed
Rated torque	Nm	6.2	8.0
Rated speed	r/min	1500	
Rated current	Arms	5.3	
Stator outer diameter	mm	122	
Stator inner diameter	mm	63.6	
Air-gap length	mm	0.4	
Stack length	mm	55	
Magnet grade	-	N35SH	
Steel grade	-	35CS440	
PM usage	mm ³	24420	

constraint ranges are assigned in order to avoid the conflicts and errors during the geometric modeling process. The optimization target is to maximize the average torque (T_{ave}) and minimize the torque ripple (T_{rip}), of which the corresponding weight factors are 1 and 0.5, respectively. The optimization results are shown in Fig. 9. The settings of GA are as follows: The population size, mating pool size, individual crossover probability, and mutation probability are 20, 20, 0.5, and 1, respectively. The major design parameters of the AMP-IPM and conventional IPM machines are listed in Table II.

C. Open-Circuit Performance

The air-gap flux density waveforms of the conventional IPM and AMP-IPM machines are shown in Fig. 10, and the corresponding open-circuit field distributions are plotted in Fig. 11.

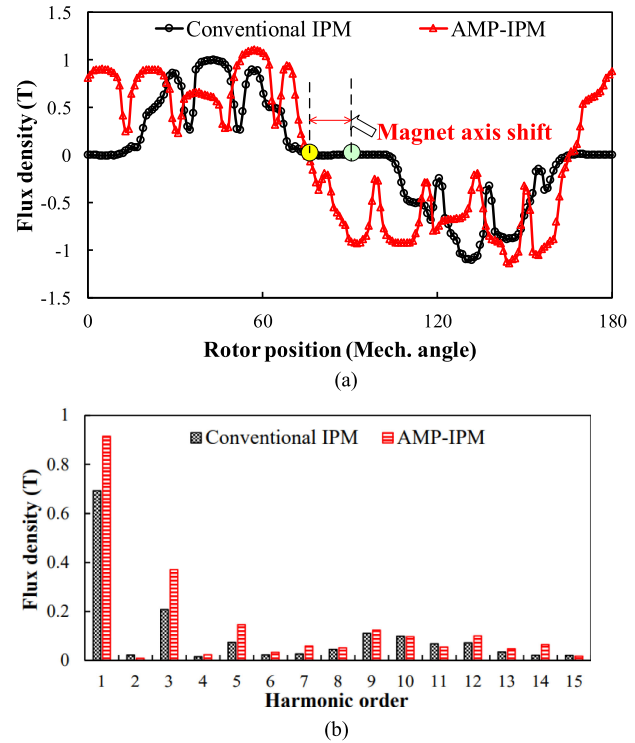


Fig. 10. Open-circuit air-gap flux density. (a) Waveforms. (b) Harmonic spectra.

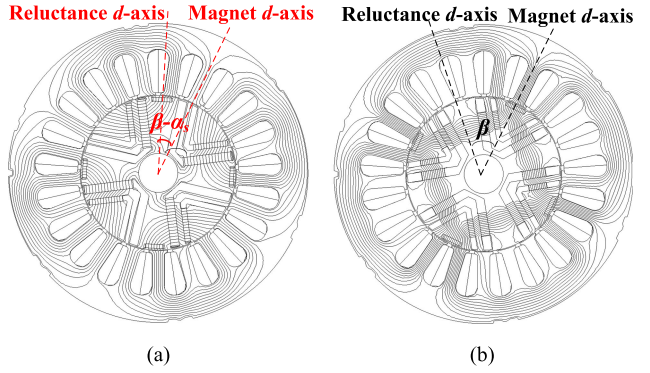
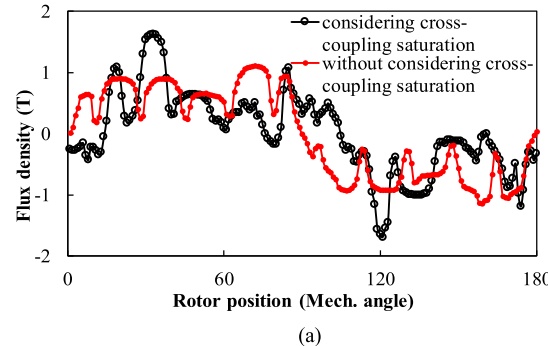


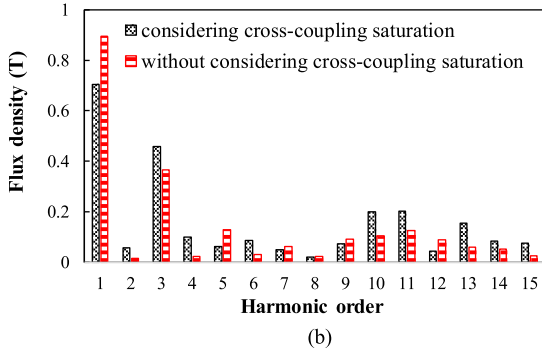
Fig. 11. Open-circuit field distributions. (a) Proposed AMP-IPM machine. (b) Conventional IPM machine.

It demonstrates that the distance between the reluctance and magnet d -axes is effectively reduced in the proposed AMP-IPM machine due to the MAS effect. Moreover, when changing the position of the magnets, the magnetic circuit varies a lot. In fact, the main flux path becomes quite shorter in the case of AMP-IPM machine. Meanwhile, due to the reduced magnet pieces in the proposed design, the magnetic reluctances for the main flux path become smaller. As a result, the fundamental flux density is significantly improved.

On the other hand, the magnet torque is mainly contributed by the fundamental air-gap flux density due to the PM excitation when considering the on-load cross-coupling saturation effect. Thus, the actual air-gap flux density due to the magnets is extracted by the frozen permeability method, as illustrated in Fig. 12. In this case, the influence of cross-coupling saturation



(a)



(b)

Fig. 12. Comparison of open-circuit air-gap flux density with or without considering cross-coupling saturation. (a) Waveforms. (b) Harmonic spectra.

makes the PM magnetic field distorted under loaded condition, which is quite different from the open-circuit situation. From the harmonic spectra in Fig. 12(b), it can be observed that the fundamental air-gap flux density is reduced under loaded operation, resulting in the compromised magnet torque, as will be presented in the following investigation.

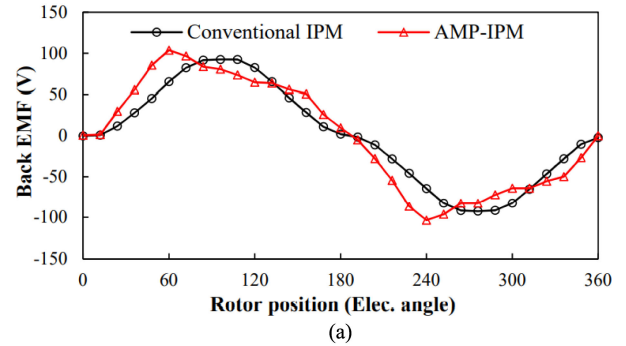
Furthermore, the open-circuit back-EMF waveforms @1500 r/min are shown in Fig. 13. It can be seen that the proposed AMP-IPM machine exhibits unbalanced and larger high-order harmonics, as evidenced in Fig. 13(b). This is mainly attributed to the asymmetric rotor PM design.

The cogging torque of two IPM machine is shown in Fig. 14. It can be observed that the peak cogging torque of the proposed is slightly higher due to the asymmetric structure design. Nonetheless, as can be observed in Fig. 12(b), when considering cross-coupling saturation, the 5th and 7th harmonics in the actual air-gap flux density produced to the magnets which mainly contributes to the torque ripple are reduced in Fig. 12. Thus, the resultant torque ripple of the AMP-IPM machine is lower than that of the conventional IPM machine.

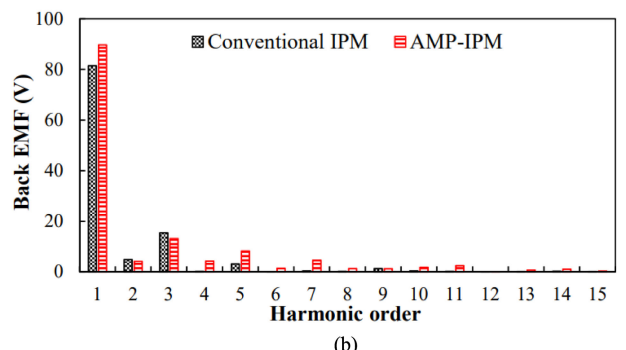
D. On-Load Performance

The d -axis and q -axis armature fields are plotted in Figs. 15 and 16, in which the reluctance axis can be identified clearly. They demonstrate that the reluctance d - and q -axes remain unchanged. Thus, the proposed AMP-IPM machine can be conveniently designed by setting an appropriate k_{het} to realize the optimal MAS effect and hence torque improvement.

The steady-state PM and reluctance torque components of conventional IPM and proposed AMP-IPM machines under

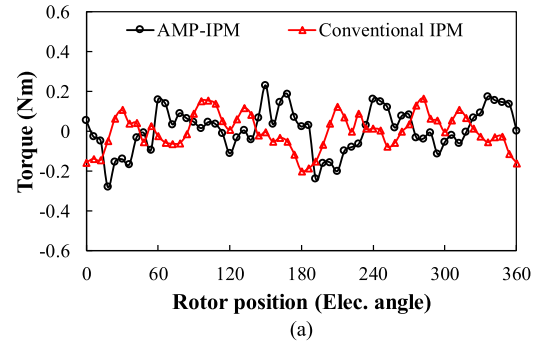


(a)

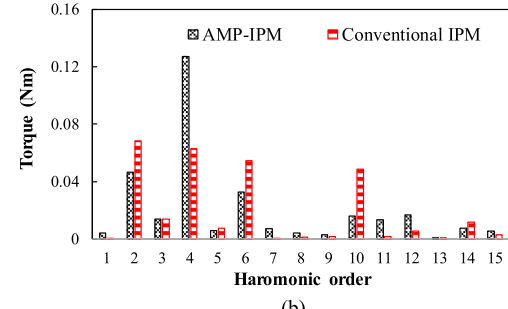


(b)

Fig. 13. Open-circuit back-EMF. (a) Waveforms. (b) Harmonic spectra.



(a)



(b)

Fig. 14. Cogging torques of two IPM machines. (a) Waveforms. (b) Harmonic spectra.

maximum torque per ampere (MTPA) control are extracted as shown in Fig. 17 below. It can be clearly visualized that under the same PM usage, the effective magnet and reluctance torques contributed to the total torque in the proposed AMP-IPM machine are both higher than those of the conventional counterpart, which is mainly due to the pronounced

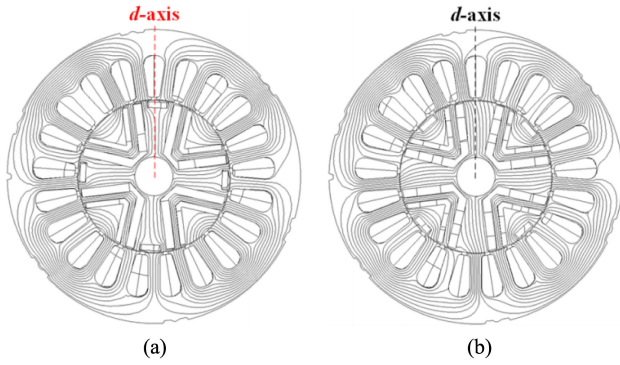


Fig. 15. Armature field distributions (*d*-axis). (a) Proposed AMP-IPM machine. (b) Conventional IPM machine.

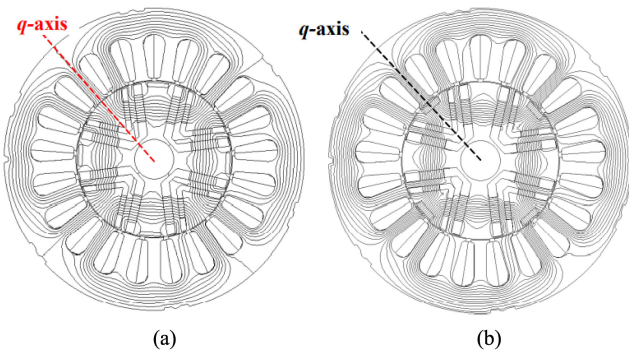


Fig. 16. Armature field distributions (*q*-axis). (a) Proposed AMP-IPM machine. (b) Conventional IPM machine.

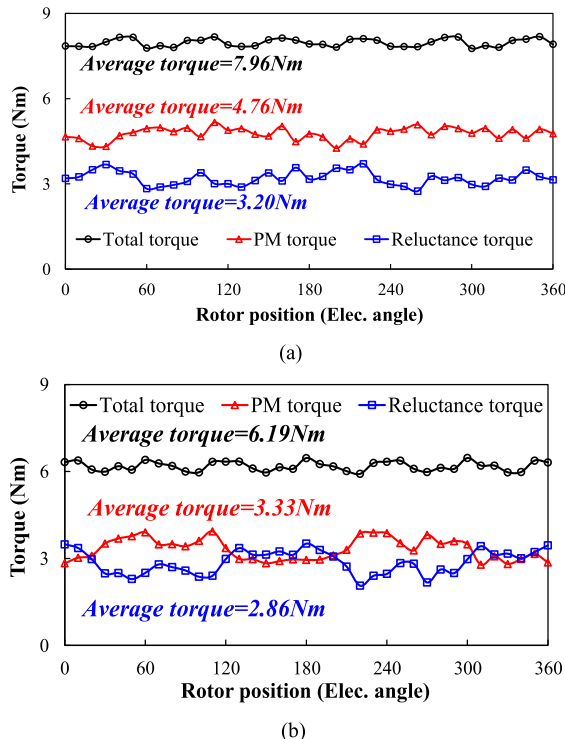


Fig. 17. Average torque of PM torque and reluctance torque. (a) Proposed AMP-IPM machine. (b) Conventional IPM machine. @ 7.5 A.

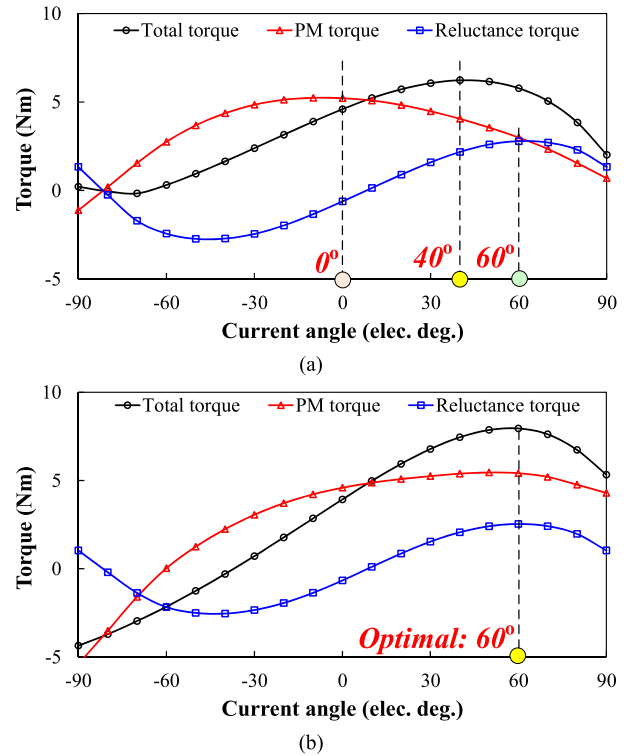


Fig. 18. Torque against current angle curves. (a) Conventional IPM machine. (b) Proposed AMP-IPM machine @ 7.5 A.

MAS effect of the proposed design. The torque characteristics of the conventional IPM and AMP-IPM machines are shown in Figs. 18 and 19, respectively. From the torque against current angle characteristics in Fig. 18, it shows that the alignment between the optimal phase current angles for the magnet and reluctance torques confirms the feasibility of the MAS effect in the proposed AMP-IPM design, resulting in the torque capability improvement over the conventional design. Besides, Fig. 19(a) suggests that the proposed AMP-IPM shows 28.9% higher average torque and 40.9% lower torque ripple than the conventional counterpart at rated-load. From Fig. 19(b), it shows that the torque capability of the AMP-IPM machine is basically higher than that of the conventional case with same PM usage.

E. Torque and Power Characteristics

The flux-weakening characteristics of the two IPM machines are evaluated. Fig. 20 illustrates the torque and power against the speed curves of the two IPM machines. It demonstrates that the proposed AMP-IPM machine can provide higher torque and output power in the low-speed region, while the flux-weakening ability of the conventional IPM machine in the high-speed region is better than that of the proposed AMP-IPM machine. This is due to the higher flux weakening coefficient of the conventional IPM machine. That is also to say, the lower flux linkage and back-EMF of the conventional IPM machine at high-speed operation is helpful for the speed range extension under the limited voltage rating of the inverter.

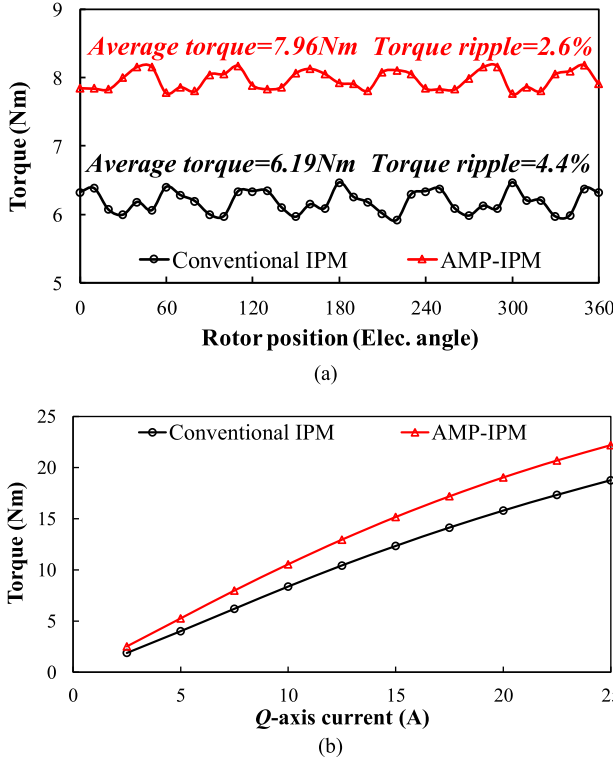


Fig. 19. Torque characteristics. (a) Steady-state torque waveforms @ MTPA operation. (b) Torque against current waveforms.

TABLE III
PARAMETERS OF CONVENTIONAL IPM AND PROPOSED AMP-IPM MACHINES

Items	Unit	Conventional	Proposed
L_d	mH	13.82	15.50
L_q	mH	29.25	28.36
N_r	-	4	4
u_{lim}	V	200	200
i_{lim}	A	7.5	7.5
ψ_m	Wb	0.275	0.3413
k_{fw}	-	0.38	0.34
ω_{base}	rad/s	170.2	138.6
n_{base}	r/min	1625	1330

When adopting the asymmetric-magnetic-pole design, the magnetic circuit varies a lot. In fact, as can be illustrated in Fig. 15 and 16, the d -axis and q -axis magnetic flux paths become quite shorter in the case of AMP-IPM machine. For both machines, the position of the d -axis reluctance does not change, which means that the q -axis reluctance is similar. However, due to the change of the PM d -axis magnetic flux path, the d -axis reluctance of the AMP machine becomes smaller, leading to the increase of the inductance of d -axis. The related parameters of conventional IPM and proposed AMP-IPM machines are shown in Table III. It should be noted that a flux-weakening factor k_{fw} that characterizes the capability extending the speed range above the base speed can be defined as [26]

$$k_{fw} = \frac{L_d i_{lim}}{\psi_{pm}} \quad (3)$$

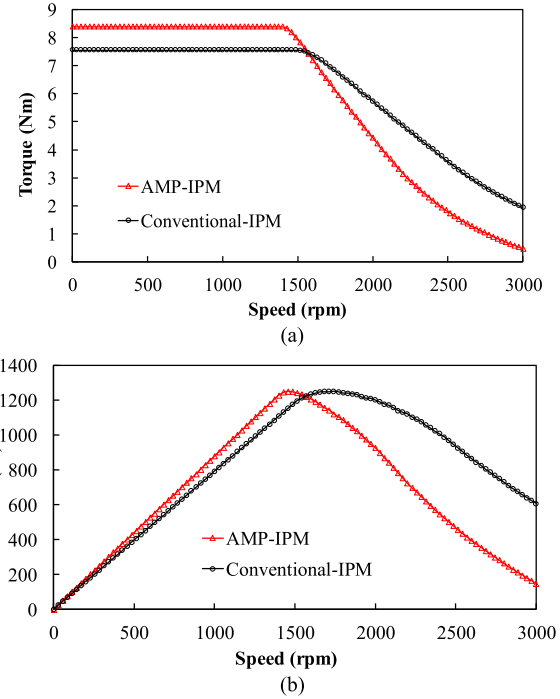


Fig. 20. (a) Torque against speed curves. (b) Power against speed curves.

where i_{lim} , L_d , and ψ_{pm} are the maximum phase current, d -axis inductance, and PM flux linkage, respectively.

The base speed ω_{base} , which stands for the dividing point between the constant-torque and constant-power operating regions, can be expressed by

$$\omega_{base} = \frac{u_{lim}}{N_r \sqrt{(\psi_m)^2 + (L_d i_{lim})^2}} \quad (4)$$

where u_{lim} , i_{lim} , L_d , and N_r are the maximum phase voltage, phase current, d -axis inductance, and rotor pole number; Ψ_m is the phase flux-linkage. The d -axis inductance of the proposed AMP-IPM machine is bigger than that of the conventional IPM machine, so that the rated speed of the proposed topology turns out to be a bit smaller than the conventional topology.

F. Efficiency and Loss Characteristics

The efficiency against speed curve of the two IPM machines at the rated-load state is plotted in Fig. 21. It demonstrates that the proposed AMP-IPM machine exhibits higher efficiency under rated load operation. In addition, the efficiency maps are illustrated in Fig. 22. It shows that the proposed AMP-IPM machine shows larger high efficiency region due to its torque improvement, albeit of the compromised flux-weakening capability. This phenomenon can be also reflected and explained by the loss maps as illustrated in Fig. 23. Obviously, the low-speed copper loss in the proposed AMP-IPM machine tends to be relatively lower than the conventional IPM one, while the higher iron loss occurs in the high-speed light-load for the proposed structure due to its relatively high air-gap field harmonics caused by AMP structure. In fact, it should be mentioned that the speed range of the proposed AMP-IPM machine will be optimized by using

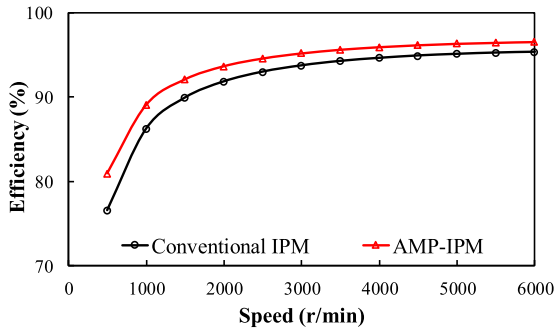


Fig. 21. Comparison of efficiency versus speed curves @ MPTA operation (rated load).

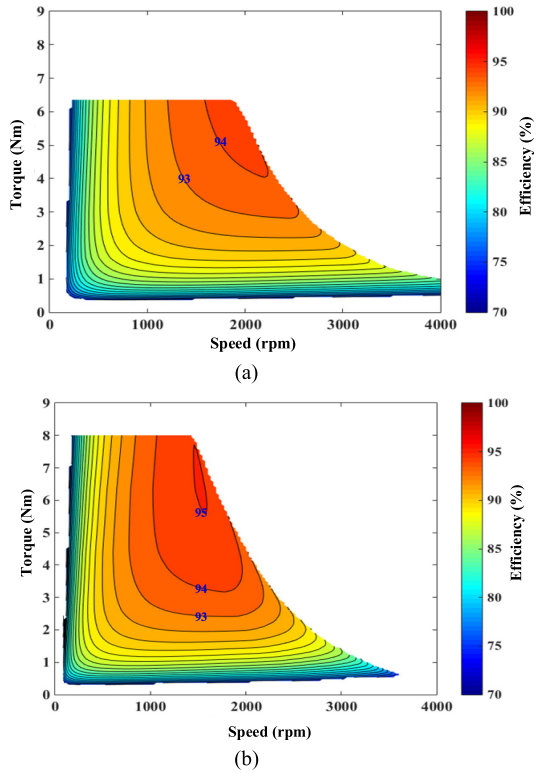


Fig. 22. Comparison of efficiency maps. (a) Conventional IPM machine. (b) Proposed AMP-IPM machine. (DC-link voltage = 200V).

better slot/pole optimization or other appropriate asymmetric PM structure.

IV. EXPERIMENTAL VALIDATION

An AMP-IPM machine prototype is manufactured to experimentally verify the foregoing theoretical analyses. The prototype and test rig are shown in Fig. 24. The test platform for measuring the machine on-load performance is shown in Fig. 24(c). The load torque is provided by the servo machine, and the torque and speed data are collected by HBM's T20WN torque and speed sensor. A conventional PM machine serves as a generator load for the proposed AMP-IPM machine. The finite element (FE)-predicted and measured back-EMF characteristics are shown in Fig. 25. The observed mismatch is mainly due to the manufacturing tolerance, mechanical loss, and the ignorance

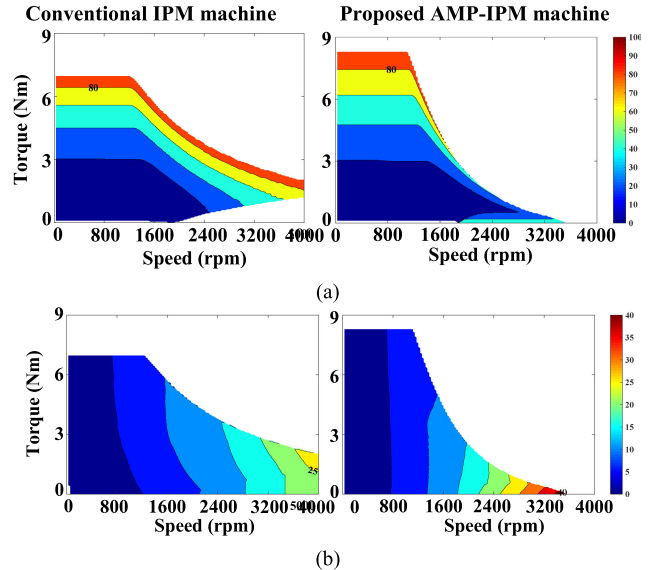


Fig. 23. Comparison of loss maps. (a) Copper loss. (b) Iron loss.

of the end-effect in FE prediction. In addition, Fig. 26 shows the FE predicted and measured torque versus current angle subject to different phase current. It should be noted the current angle in the test is designated as the angle between the phase current and the PM d -axis. Besides, Fig. 27 shows the FE predicted and measured torque against current curves. The difference between simulated and measured results is mainly due to the fact that the mechanical tolerance is not considered in the FE analyses. In addition, the asymmetric rotor pole leads to the increase of flux leakage at the end [27]. Overall, good agreement between FE predictions and measurements confirms the aforementioned theoretical and FE analyses.

V. CONCLUSION

This article proposes a novel AMP-IPM machine by combining dual-layer reluctance and flat-type rotor PM structures. The operating principle of the proposed AMP-IPM design is analyzed with reference to the conventional IPM machine. It can be found that the MAS effect is achieved in the proposed AMP-IPM machine due to the “asymmetric PM arrangement,” resulting in the fact that the PM and reluctance torques maximize at the same current angle. Besides, the electromagnetic characteristics of the two IPM machines are compared. It shows that the proposed AMP-IPM provides 28.9% higher average torque, 40.9% lower torque ripple, and higher peak efficiency than the conventional counterpart at rated-load state. Besides, it can be found that the proposed AMP-IPM machine shows larger high efficiency region due to its torque improvement, albeit of the compromised flux-weakening capability. Further, the proposed AMP-IPM machine can output higher torque and power in the low speed region, thus generating greater total torque and overload capacity. The theoretical analyses have been verified by experiments on an AMP-IPM machine prototype, which confirm the feasibility of the proposed AMP-IPM design for the performance improvement.

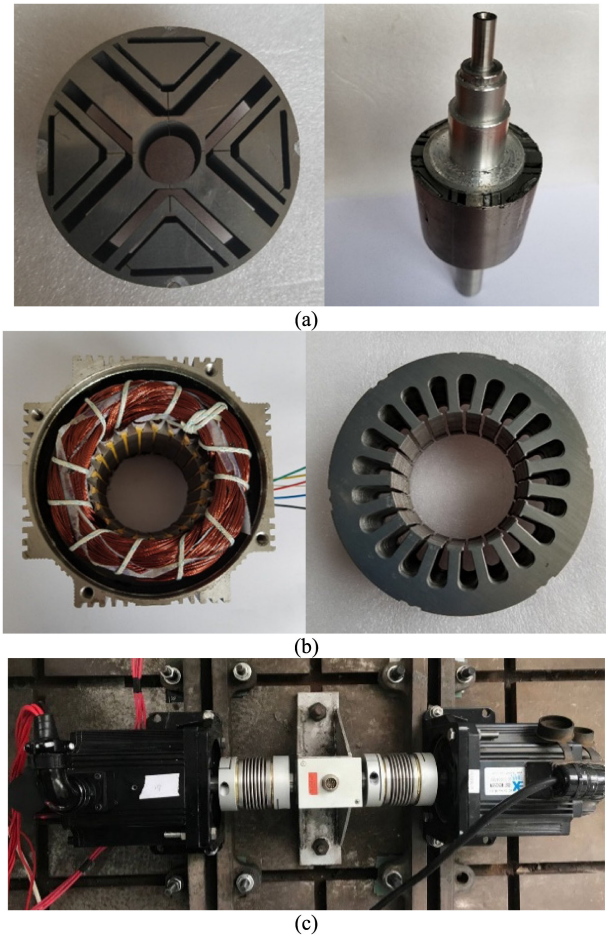


Fig. 24. Prototype and test rig. (a) Rotor. (b) Stator. (c) Test rig.

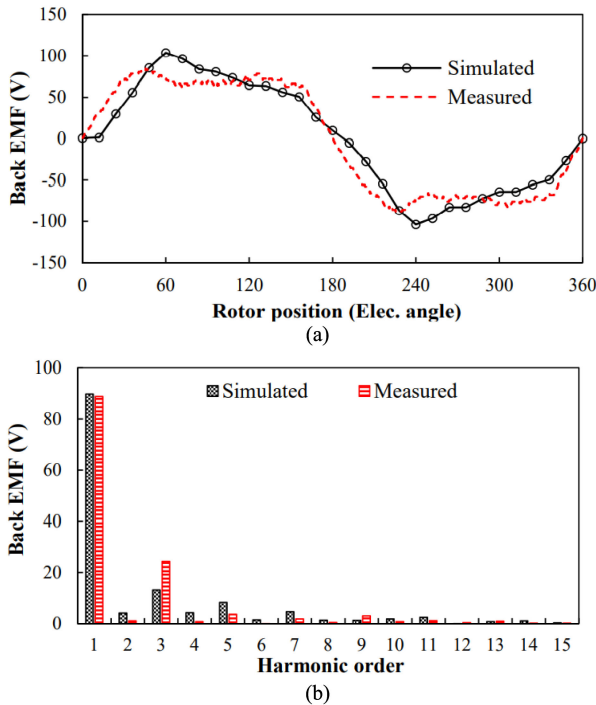


Fig. 25. Comparison of FE and measured back-EMFs @ 1500 r/min. (a) Waveform. (b) Harmonic spectra.

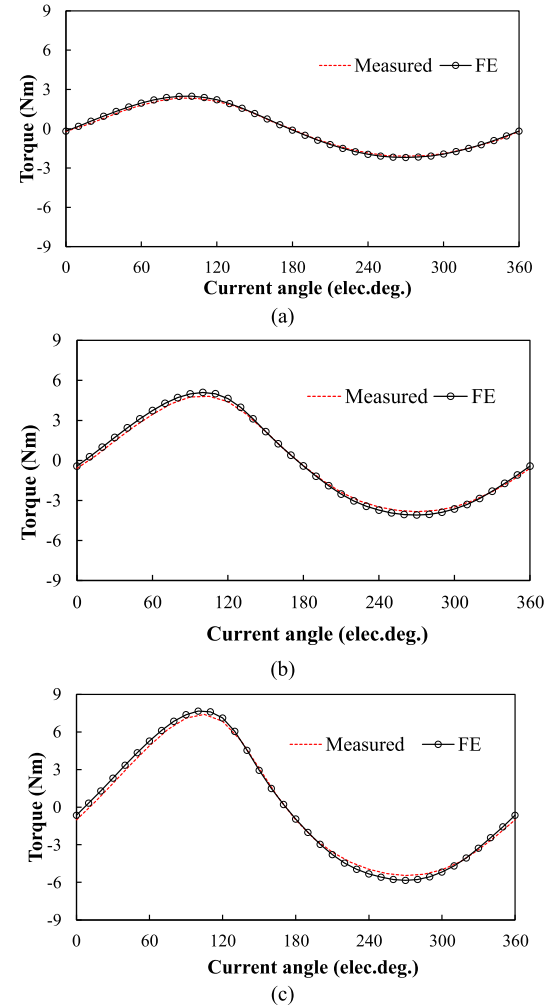


Fig. 26. Comparison of FE and measured torques against current angle. $I_s =$ (a) 2.5 A. (b) 5 A. (c) 7.5 A.

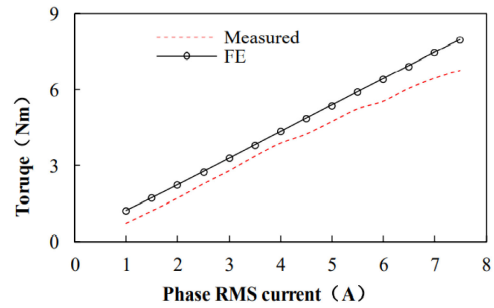


Fig. 27. Comparison of FE and measured torques against current curves.

APPENDIX

QUANTITATIVE COMPARISON OF THE PROPOSED AMP-IPM MACHINE WITH THE EXISTING ASYMMETRIC IPM MACHINES

A quantitative comparison of the proposed AMP-IPM machine with the other two types of asymmetrical IPM machines: the spoke-type [14] and V-type IPM [15] machines. The corresponding machine topologies are shown in Fig. 28. In order to perform the comparison fairly, these machines are assumed with identical stator structure, outer diameter, split ratio, stack length,

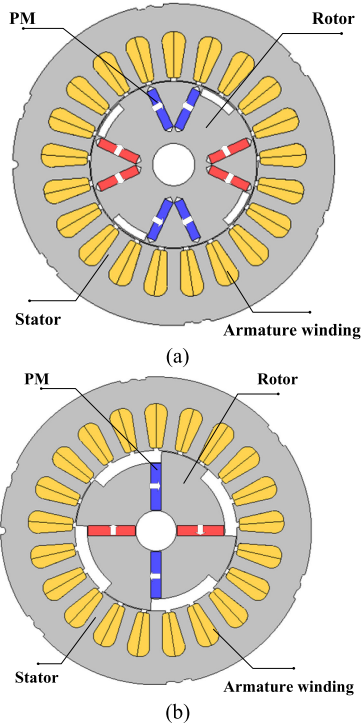


Fig. 28. AMP-IPM machine topologies. (a) V-type AMP-IPM machine. (b) Spoke-type AMP-IPM machine.

TABLE IV
MAIN DESIGN SPECIFICATIONS OF THE V-TYPE AND SPOKE-TYPE
IPM MACHINE

Parameters	Asymmetric V-type	Asymmetric spoke-type
Rated speed (r/min)	1500	
Outer diameter of stator (mm)	122	
Split ratio	0.52	
Air-gap length (mm)	0.4	
Active stack length (mm)	55	
Rated current (Arms)	5.3	
Turns of winding per phase	30	
Magnet thickness (mm)	3.6	
Magnet grade	N35SH	
Steel material	35CS440	

air-gap length, and rated current. Furthermore, the double-layer armature windings are employed for these three topologies. The main design specifications of the three machines are listed in Table IV.

The torque against current angle curves of the two asymmetric IPM machines for comparison are shown in Fig. 29. From the observation on the optimal current angles for the magnet, reluctance, as well as resultant torques, the “V-type” asymmetric IPM machine shows slightly greater RAS effect than the spoke-type structure, which is mainly attributed to the fact that the flux path produced by the magnets is affected by the additional airspace in the case of the spoke-type machine. Overall, the MAS effect of the proposed AMP-IPM design is more pronounced than the asymmetric IPM machines, which well confirms its advantage in terms of the torque enhancement.

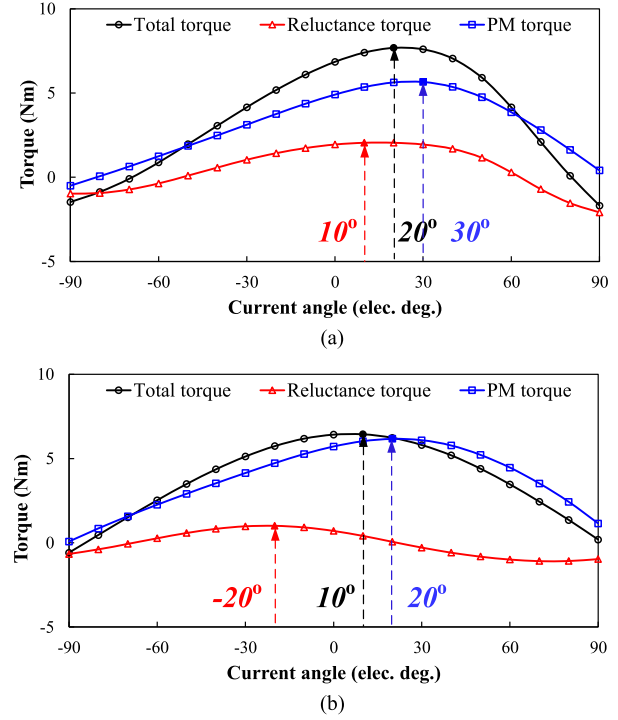


Fig. 29. Torque against current angle curves. (a) V-type AMP-IPM machine. (b) Spoke-type AMP-IPM machine @ 7.5 A.

TABLE V
COMPARISON OF KEY PERFORMANCE METRICS OF THE THREE INVESTIGATED
MACHINES @ OPEN-CIRCUIT OR RATED-LOAD STATES

Items	Unit	Proposed AMP-IPM	Asymmetric V-type	Asymmetric spoke-type
Average torque	N·m	7.96	7.68	6.44
Magnet usage	mm ³	24420	24640	16280
Torque/PM volume	N·m/cm ³	0.326	0.312	0.396
UR_{pm}	%	100	99	98
UR_r	%	100	99	40

The key torque characteristics and magnet usages of the three machines are compared as listed in Table V. It should be mentioned the torque utilization ratio (UR) can be defined as [15]

$$\text{For magnet torque: } UR_{pm} = \frac{T_{u,pm}}{T_{\max,pm}} \quad (5)$$

$$\text{For reluctance torque: } UR_r = \frac{T_{u,r}}{T_{\max,r}} \quad (6)$$

where $T_{u,pm}$ and $T_{u,r}$ are the utilized magnetic torque and the utilized reluctance torque that contribute to the maximum resultant torque, respectively. $T_{\max,pm}$ and $T_{\max,r}$ are the peak values of each torque component. It can be observed from Table V that the proposed AMP-IPM machine shows the best torque utilization ratio due to its most pronounced MAS effect. Meanwhile the highest cost-effectiveness, i.e., its highest torque per magnet volume characteristics, can be found in the case of spoke-type IPM machine. Overall, it can be summarized that the asymmetric IPM machines can be recognized as potential alternatives to conventional IPM machines, which are favorable for cost-sensitive applications requiring high torque density.

REFERENCES

- [1] A. M. El-Refaie, "Motors/generators for traction/proulsion applications: A review," *IEEE Veh. Technol. Mag.*, vol. 8, no. 1, pp. 90–99, Mar. 2013.
- [2] Z. Q. Zhu and D. Howe, "Electrical machines and drives for electric, hybrid, and fuel cell vehicles," *Proc. IEEE*, vol. 95, no. 4, pp. 746–765, Apr. 2007.
- [3] K. Chau, C. C. Chan, and C. Liu, "Overview of permanent-magnet brushless drives for electric and hybrid electric vehicles," *IEEE Trans. Ind. Electron.*, vol. 55, no. 6, pp. 2246–2257, May 2008.
- [4] H. Zhang, W. Hua, Z. Wu, and X. Zhu, "Design considerations of novel modular-spoke-type permanent magnet machines," *IEEE Trans. Ind. Appl.*, vol. 54, no. 5, pp. 4236–4245, May 2018.
- [5] A. S. Thomas, Z. Q. Zhu, and G. W. Jewell, "Comparison of flux switching and surface mounted permanent magnet generators for high-speed applications," *IET Elect. Syst. Transp.*, vol. 1, no. 3, pp. 111–116, Sep. 2011.
- [6] I. Boldea, L. N. Tutelea, L. Parsa, and D. Dorrell, "Automotive electric propulsion systems with reduced or no permanent magnets: An overview," *IEEE Trans. Ind. Electron.*, vol. 61, no. 10, pp. 5696–5711, Jan. 2014.
- [7] Z. Q. Zhu, W. Q. Chu, and Y. Guan, "Quantitative comparison of electromagnetic performance of electrical machines for HEVs/EVs," *CES Trans. Elect. Mach. Syst.*, vol. 1, no. 1, pp. 37–47, Jul. 2017.
- [8] Z. S. Du and T. A. Lipo, "Efficient utilization of rare earth permanent-magnet materials and torque ripple reduction in interior permanent-magnet machines," *IEEE Trans. Ind. Appl.*, vol. 53, no. 4, pp. 3485–3495, Jul./Aug. 2017.
- [9] S. S. Maroufian and P. Pillay, "PM assisted synchronous reluctance machine design using alnico magnets," in *Proc. IEEE Int. Electric Machines Drives Conf.*, Miami, FL, USA, May 2017, pp. 1–6.
- [10] M. Xu, G. Liu, and W. Zhao, "Torque ripple improvement for ferrite-assisted synchronous reluctance motor by using asymmetric flux-barrier arrangement," in *Proc. IEEE Int. Magn. Conf.*, Singapore, Apr. 2018, p. 1.
- [11] B. J. Chalmers, R. Akmese, and L. Musaba, "Design and field-weakening performance of permanent magnet/reluctance motor with two-part rotor," *IEE Proc. Elec. Power Appl.*, vol. 145, no. 2, pp. 133–139, Mar. 1998.
- [12] P. Winzer and M. Doppelbauer, "A hybrid permanent magnet and wound field synchronous machine with displaced reluctance axis capable of symmetric four quadrant operation," in *Proc. 18th Eur. Conf. Power Electron. Appl.*, Karlsruhe, 2016, pp. 1–11.
- [13] W. Zhao, T. A. Lipo, and B. Kwon, "Optimal design of a novel asymmetric rotor structure to obtain torque and efficiency improvement in surface inset PM motors," *IEEE Trans. Magn.*, vol. 51, no. 3, Mar. 2015, Art. No. 8100704.
- [14] Y. Xiao, Z. Q. Zhu, J. T. Chen, D. Wu, and L. M. Gong, "A novel spoke-type asymmetric rotor interior PM machine," in *Proc. IEEE Energy Convers. Congr. Expo.*, Detroit, MI, USA, Oct. 2020, pp. 4050–4057.
- [15] W. Zhao, F. Zhao, T. A. Lipo, and B. I. Kwon, "Optimal design of a novel V-type interior permanent magnet motor with assisted barriers for the improvement of torque characteristics," *IEEE Trans. Magn.*, vol. 50, no. 11, Dec. 2014, Art. no. 8104504.
- [16] R. Thike and P. Pillay, "Mathematical model of an interior PMSM with aligned magnet and reluctance torques," *IEEE Trans. Transp. Electricif.*, vol. 6, no. 2, pp. 647–658, Jun. 2020.
- [17] H. Yang *et al.*, "Novel reluctance axis shifted machines with hybrid rotors," in *Proc. IEEE Energy Convers. Congr. Expo.*, Cincinnati, OH, USA, Oct. 2017, pp. 2362–2367.
- [18] W. Zhao, H. Shen, T. A. Lipo, and X. Wang, "A new hybrid permanent magnet synchronous reluctance machine with axially sandwiched magnets for performance improvement," *IEEE Trans. Energy Convers.*, vol. 33, no. 4, pp. 2018–2029, Dec. 2018.
- [19] Y. Li, D. Bobba, and B. Sarlioglu, "Design and optimization of a novel dual-rotor hybrid PM machine for traction application," *IEEE Trans. Ind. Electron.*, vol. 65, no. 2, pp. 1762–1771, Feb. 2018.
- [20] J. Y. Alsawalhi and S. D. Sudhoff, "Design optimization of asymmetric salient permanent magnet synchronous machines," *IEEE Trans. Energy Convers.*, vol. 31, no. 4, pp. 1315–1324, Dec. 2016.
- [21] W. Zhao, D. Chen, T. A. Lipo, and B. Kwon, "Performance improvement of ferrite-assisted synchronous reluctance machines using asymmetric rotor configurations," *IEEE Trans. Magn.*, vol. 51, no. 11, Nov. 2015, Art. No. 8108504.
- [22] Y. Xiao *et al.*, "A novel asymmetric interior permanent magnet machine for electric vehicles," *IEEE Trans. Energy Convers.*, vol. 36, no. 3, pp. 2404–2415, Sept. 2021, doi: [10.1109/TEC.2021.3055260](https://doi.org/10.1109/TEC.2021.3055260).
- [23] Y. Xiao, Z. Q. Zhu, J. T. Chen, D. Wu, and L. M. Gong, "A novel asymmetric rotor interior PM machine with hybrid-layer PMs," in *Proc. IEEE Energy Convers. Congr. Expo.*, Detroit, MI, USA, Oct. 2020, pp. 4029–4035.
- [24] Y. Li, H. Yang, H. Lin, S. Fang, and W. Wang, "A novel magnet-axis-shifted hybrid permanent magnet machine for electric vehicle applications," *Energies*, vol. 12, no. 4, Feb. 2019, Art. no. 641.
- [25] H. Yang, W. Wang, H. Lin, Z. Q. Zhu, S. Lyu, and S. Niu, "A novel hybrid-pole interior PM machine with magnet-axis-shifting effect," in *Proc. IEEE Inter. Electr. Machines Drives Conf.*, San Diego, CA, USA, May 2019, pp. 273–279.
- [26] D. Zarko, D. Ban, and T. A. Lipo, "Design optimization of interior permanent magnet (IPM) motors with maximized torque output in the entire speed range," in *Proc. Eur. Conf. Power Electron. Appl.*, 2005, pp. 1–10.
- [27] H. Hua, Z. Q. Zhu, A. Pride, R. P. Deodhar, and T. Sasaki, "Comparison of end effect in series and parallel hybrid permanent-magnet variable-flux memory machines," *IEEE Trans. Ind. Appl.*, vol. 55, no. 3, pp. 2529–2537, May/Jun. 2019.